RSC Advances

ROYAL SOCIETY OF CHEMISTRY

www.rsc.org/advances

Graphical Abstract

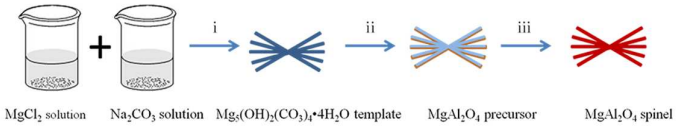

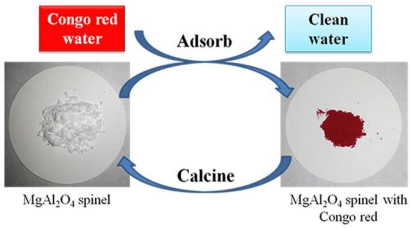

Hierarchical and porous $MgAl_2O_4$ spinel with excellent absorption performance has been synthesized via a facile hard template process.

Cite this: DOI: 10.1039/c0xx00000x

www.rsc.org/xxxxxx

ARTICLE TYPE

Synthesis of porous $MgAl_2O_4$ spinel and its superior performance for organic dye adsorption

Junying Tian, Peng Tian, Guiling Ning,* Hongchang Pang, Qiang Song, Hang Cheng, and Haixia Fang

Received (in XXX, XXX) Xth XXXXXXXXX 20XX, Accepted Xth XXXXXXXXX 20XX

DOI: 10.1039/b000000x

Porous $MgAl_2O_4$ spinel (MAS) has been synthesized *via* a facile hard template process with further calcination, in which hierarchical $Mg_5(OH)_2(CO_3)_4{\cdot}4H_2O$ template with high surface was used as hard template and magnesium source, and $AlCl_3{\cdot}6H_2O$ was used as alumina source. The as-prepared samples were characterized by X-ray diffraction (XRD), Fourier transform infrared spectroscopy (FTIR), scanning electron microscopy (SEM), energy dispersive X-ray (EDX), thermogravimetry analysis (TGA) and N_2 adsorption-desorption. The MAS samples showed superior adsorption performance, including rapid adsorption rate, excellent adsorption capacity and good reusability for removal of Congo red (CR) from aqueous solution. The superior performance could be ascribed to the strong interaction between the MAS samples and CR, as well as the hierarchical porous structure and the high specific surface area of the samples. The maximum adsorption capacity of the MAS samples for CR was nearly 845 mg g^{-1}, which is higher than most of the previously reported adsorbents. The CR removal process was found to follow the pseudo-second-order rate equation and the Sips adsorption model.

1. Introduction

Nowadays, dyes and organic waste have become one of the main pollution sources of ground water and surface water.[1] Many of them are human carcinogen, whereas, have been widely used in industry. Therefore, the remaining organic dyes must be removed before they are mixed up with any water resource. Adsorption has been recognized as one popular treatment method to remove organic dyes from colored effluents because of the simplicity, high efficiency and low cost of the adsorbent.[2-7] Nevertheless, the application of traditional adsorbent is affected by several restrictions, such as limited adsorption capacity, low adsorption rate and poor reusability. Therefore, preparation of the adsorbent with high adsorption capacity and good reusability has become the focus of recent research.

Magnesium aluminate ($MgAl_2O_4$) spinel (MAS) has been extensively used as a dye adsorbent, catalyst or catalyst support, an active element in humidity sensors and an excellent transparent ceramic material for high-temperature arc-enclosing envelops, because of its unique properties, such as high melting point (2,135 °C), low dielectric constant, chemical inertness, excellent optical properties, good mechanical strength, low thermal expansion and good catalytic properties.[8-17] For many of its applications, especially as a dye adsorbent, catalyst support and catalysts by itself, high specific surface area is greatly desired. Several chemical synthetic methods such as chemical coprecipitation[14, 15, 18-20] and sol-gel processes[8, 21-24], have been used to synthesize MAS materials with high surface area. In despite of these successes, the experimental parameters in chemical coprecipitation or sol-gel processes are often entangled, making it difficult to control the shape, morphology, and structure of the micro/nanostructured materials, and hard to synthesize the micro/nanostructured materials in large scale.

Recently, several metallic oxides have been prepared successfully by magnesium carbonate hard template route in our studies.[3, 25-27] The route is facile, inexpensive, and easily scaled-up. In this present work, MAS hierarchical structures with high surface area were prepared by a hard template process with further calcination, in which $Mg_5(OH)_2(CO_3)_4{\cdot}4H_2O$ (MCH) template with hierarchical structure was used as hard template as well as magnesium source, and $AlCl_3{\cdot}6H_2O$ was used as alumina source. Congo red, an azo anionic dye and a known human carcinogen, is widely used in dyeing, paper, rubber, and plastics industries, and commonly used as a model pollutant to investigate the dye removal ability of adsorbents.[4,5,28-32]Furthermore, as a representative demonstration for dye adsorption, MAS was used to adsorb CR. The as-obtained MAS powder possessed a high adsorption capacity (840 mg g^{-1}) and good reusability. The properties of as-prepared MAS, including the simple preparation, high adsorption rate, ultrahigh adsorption capacity and good reusability, make it be potential for application in environmental remediation.

2. Experimental

2.1 Preparation of MAS powder

All reagents used during the process were AR, unless otherwise noted. Schematic diagram of the synthesis of the MAS samples is

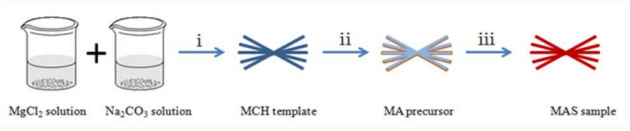

Scheme1 Schematic diagram of the formation of MAS samples.

exhibited in Scheme 1. In the first step, the aqueous $MgCl_2 \cdot 6H_2O$ solution (50 ml, 1 M) and aqueous Na_2CO_3 solution (100 ml, 0.5 M) were heated to 80 °C. Then, the hot $MgCl_2 \cdot 6H_2O$ solution was added into vigorously stirred hot Na_2CO_3 solution (in a 250 ml beaker). After 1 min, the stirring was stopped and the solution was maintained at 80 °C for 1 h to form the $Mg_5(OH)_2(CO_3)_4 \cdot 4H_2O$ (MCH) template (XRD pattern of the MCH template is shown in Fig. S1, †ESI). After that, the template was collected, filtered off, washed with water and ethanol three times respectively, and dried in a blast drying oven at 60 °C for 8 h.

In the second step, 0.466g MCH template was dispersed in 100 ml NaOH solution (0.3 M). Then 120 ml $AlCl_3 \cdot 6H_2O$ solution (0.1 M) was added to the liquid dropwise under vigorous stirring at room temperature. The formed material was collected, filtered off, washed with water and ethanol three times respectively, and dried in a blast drying oven at 60 °C for 8 h, resulting a precursor (MA precursor). In the third step, as prepared MA precursor was calcined in air at temperature of 700-1100 °C, for 4 h, to obtain the MAS sample.

In order to compare, a bulk MAS sample (B-MAS) was prepared by a coprecipitation process. Firstly, 10 ml aqueous $MgCl_2 \cdot 6H_2O$ solution (1 M) and 20 ml aqueous $AlCl_3 \cdot 6H_2O$ solution (1 M) were mix in a 400 ml baker, then, 160 ml NaOH solution (0.5 M) was added into the vigorously stirred mixed solution. After 1 min, the stirring was stopped. And the precipitation was collected, filtered off, washed with water and ethanol three times respectively, and dried in a blast drying oven at 60 °C for 8 h. Furthermore, precipitation was calcined in air at temperature of 700 °C for 4 h, to obtain the B-MAS sample.

2.2 Characterization

The crystalline phases of the as-prepared samples were identified by X-ray powder diffraction (XRD, Rigaku-DMax 2400) in reflection mode (Cu-Ka radiation) at scanning rate of 0.02 S^{-1} in the 2θ from 5 to 80°. Scanning electron microscope (SEM, JEOL-6360LV, operated at 20 kV) was used to observe the morphology, and Energy Dispersive X-Ray (EDX) analysis was conducted during SEM. A Mettler TG/SDTA851e thermogravimetric analyzer was employed to accomplish the thermogravimetry analysis (TGA) of samples at a heating rate of 10 °C min^{-1} in air. An ASAP 2020 physisorption apparatus was used to measure adsorption−desorption isotherms of the samples at 77K (temperature of liquid nitrogen). The specific surface area and the total specific volume of the pores were calculated by the BET method and BJH method, respectively. A JASCO FT/IR-4100 spectrometric analyzer was employed to measure the Fourier transform infrared (FTIR) spectra of the samples.

2.3 Evaluation of Adsorptive property and reusability

For adsorption tests, 0.1 g of as-obtained MAS powder, which was prepared by calcinating MA precursor at different temperatures, was added to 200 mL of the aqueous solution of Congo red (CR) at different initial concentrations and pH. Then the mixture was stirred continuously at room temperature. At different adsorption times, 8.0 mL of the mixture was collected and separated. The absorbance of the CR solutions were measured on UV-visible spectrophotometer (Hitachi, U-4100), and the concentrations of the solutions were evaluated by the Beer's law. A series of solutions of defined concentration were used to explore the relationship between the CR concentration and absorbance at λ=490nm. The absorbance *vs.* concentration graphs for different concentration ranges were plotted respectively (Fig. S2, †ESI), and unknown concentration was calculated from the corresponding equations. Detail information of the CR was listed in the Table S1 (†ESI).

After adsorption, the adsorbent was collected, filtered off, washed with ethanol two times, and dried in a blast drying oven at 60 °C for 8 h. Then, the adsorbent was calcined in air at temperature of 700 °C for 1h, to obtain the regeneration powder (marked 2-MAS). This process was conducted again on the 2-MAS powder to obtain the second regeneration powder (marked 3-MAS), again. The crystalline phases and the surface area of as-obtained MAS powder, 2-MAS powder and 3-MAS powder were compared. Moreover, adsorptive property of them was evaluated.

3. Result and discussion

3.1 Characterization of MAS

The XRD patterns for MAS with different calcining temperature are shown in Fig. 1. All the diffraction peaks can be indexed to cubic spinel-structured $MgAl_2O_4$ (JCPDS Card No. 77-1203). The crystallization of the spinel phase can be clearly observed at 700 °C. And diffraction peaks become stronger with the increasing calcining temperature. This indicates that the spinel phase has formed in the calcined sample at 700 °C-1100 °C. The EDX pattern of MAS sample calcined at 1100 °C shown in Fig. S3 (†ESI) reveals that the chemical compositions of as-prepared sample are consistent with the $MgAl_2O_4$ spinel.

The nitrogen adsorption-desorption isotherms for the samples of MAS prepared at 700 °C to 1100 °C are shown in Fig. 2 (700 °C and 1100 °C) and Fig. S4 (800 °C, 900 °C and 1000 °C, †ESI). The isotherms can be classified as type II and H3 type hysteresis for all samples (according to the IUPAC classification). The isotherm curves showed that micropores (<2 nm), mesopores (2−50 nm), and macropores (>50 nm) coexisted in the as-prepared MAS， suggesting that the structures of as-obtained MAS samples were hierarchical and porous. The results for the specific surface area and total specific volume of the pores (at $P/P_o = 0.95$) are shown in Table 1. The specific surface area and total specific volume of the pores of the samples decreased with the calcination temperature, because of the shrink of the samples at the high calcination temperature. Several previous works have prepared MAS samples with higher surface area,[8, 33-35] even then, the specific surface area of as-prepared samples are high, and our synthesis route is not inferior to many of them base on the hierarchical porous structure of prepared samples and affordable of the route (cheap raw material and mild synthesis conditions).

In order to obtain information of forming process of MAS, SEM and IR spectra were used to detect the features of MCH template, MA precursor and MAS sample. Meanwhile, TG analysis was

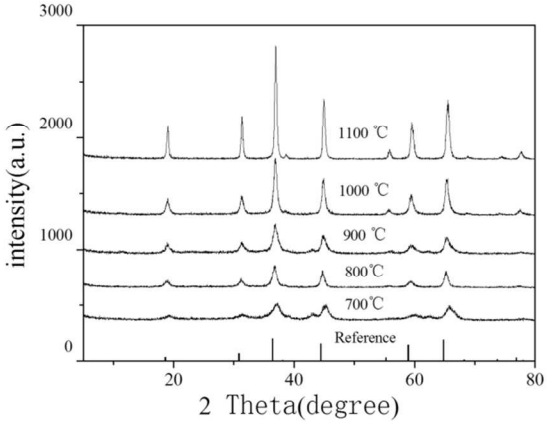

Fig. 1 Powder XRD patterns of MAS with different calcining temperatures (700-1100 °C) and reference MAS (JCPDS Card No. 77-1203).

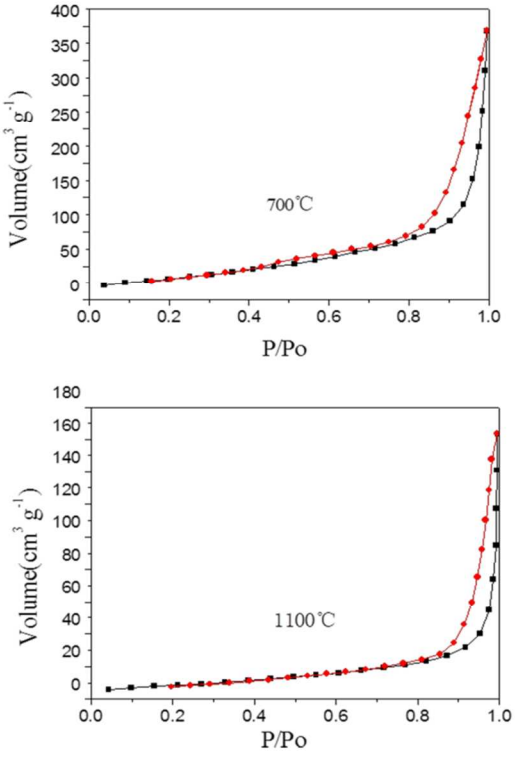

Fig. 2 N_2 ad/desorption isotherms of samples calcined at 700 and 1100 °C.

used to probe weight loss of MA precursor in the calcinations process. The SEM images of the MCH template, MA precursor and MAS sample calcined at 1100 °C are shown in Fig. 3. As can be seen, the hierarchical structure of the MCH template has been retained in the MA precursor and MAS sample. The particles were hierarchical, porous and made up of a number of microsheets, which was consistent with the high specific surface area of the samples.

IR spectra of the MCH template, MA precursor and MAS calcined at 700 °C are shown in Fig. 4a. The broad OH band around 3400 cm^{-1}, and the H_2O vibration around band 1630 cm^{-1} existed in all cases, because the MCH template and MA precursor had hydroxyl and the high surface area of these samples results in adsorption of water from the atmosphere. It is noteworthy that, there were bands at 1115 cm^{-1}, 1428 cm^{-1} and 1482 cm^{-1} associating with stretching of the CO_3^{2-} groups, and weak bands at 794 cm^{-1}, 855 cm^{-1} and 885 cm^{-1} associating with bending of the CO_3^{2-} groups in the MCH template,[36,37] while there was not any band at the same wavenumbers in the other samples. It indicated that the MCH template may had transformed to $Mg(OH)_2$ in the strong alkaline solution of the preparation process. For the MA precursor, the transmittance bands noted at 532 cm^{-1}, 778 cm^{-1} and 993 cm^{-1} correspond to the bending and stretching modes of the Al-O and Mg-O.[38] Moreover, the characteristic absorption peaks at 689 cm^{-1} and at 528 cm^{-1} of MAS were attributed to the AlO6 groups, which built up the MAS and indicated the formation of MAS powders.[9]

Table 1 The results for the surface area and total specific volume of as-prepared MAS samples

Calcination temperature °C	Surface area $m^2\ g^{-1}$	Total specific volume $cm^3\ g^{-1}$
700	127.9	0.845
800	111.9	0.713
900	99.1	0.717
1000	72.3	0.619
1100	30.5	0.254

TG analysis was used to investigate the thermal behavior of as-prepared MA precursor and the results are shown in Fig. 4b. The weight lose below 200 °C was mainly attribute to the removal of the water of the precursor, including bound water and adsorbed water. The weight losses near at 240 and 360 °C were about 10% and 6%, which fitted with the dehydroxylation of $Al(OH)_3$ and $Mg(OH)_2$, respectively. It indicated that the great weight loss ratios near at 240 °C and 360 °C were mainly due to dehydroxylation of $Al(OH)_3$ and $Mg(OH)_2$, respectively.

XRD pattern, SEM images and N_2 ad/desorption isotherms of the bulk MAS (B-MAS) were shown in the Fig. S5 (†ESI). As can be proved, the B-MAS had cubic spinel-structured phase, bulk morphology and porous structure. The specific surface area of the B-MAS was 73.2$m^2\ g^{-1}$, which was less than the specific surface area of the MAS samples calcined at 700 °C.

3.2 Adsorption study

It is likely that the as-prepared MAS powder would be powerful to remove organic pollutants from waste water, because of its hierarchical porous structure and high specific surface area. Here, Congo red (CR), a dye frequently used in the textile industry, was selected as a model to study the capture ability of the MAS powder to absorb the organic pollutant. When the initial concentration of CR in water was 300 mg L^{-1}, the UV-Vis absorption curves and photos of CR aqueous solution within different time are shown in Fig. 5. It can be seen that the as-synthesized MAS powder (0.5 g L^{-1}) could remove about 89% and 99% of the CR from the aqueous solution at room temperature in 5min and 120 min, respectively. The patterns of the MAS samples before and after adsorption are shown in the Fig.S6 (†ESI). As can be seen, main diffraction peaks of the MAS samples can be indexed to cubic spinel-structured $MgAl_2O_4$ (JCPDS Card No. 77-1203). And the diffraction peaks of the MAS powder became much weaker after adsorption. Moreover,

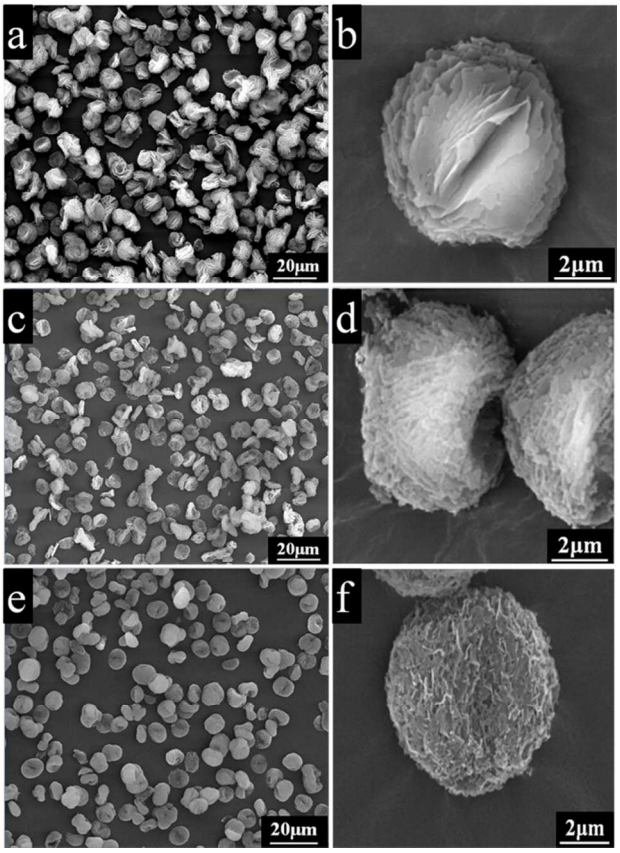

Fig. 3 SEM images of the MCH template (a,b), MA precursor (c,d) and MAS sample calcined at 1100 °C (e,f).

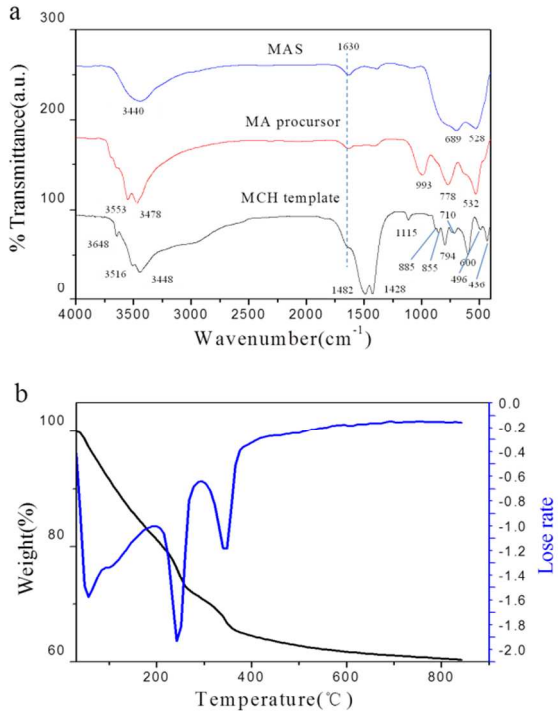

Fig. 4 (a) IR spectra for MCH template, MA precursor and MAS calcined at 700 °C. (b) TG curves for as-prepared MA precursor.

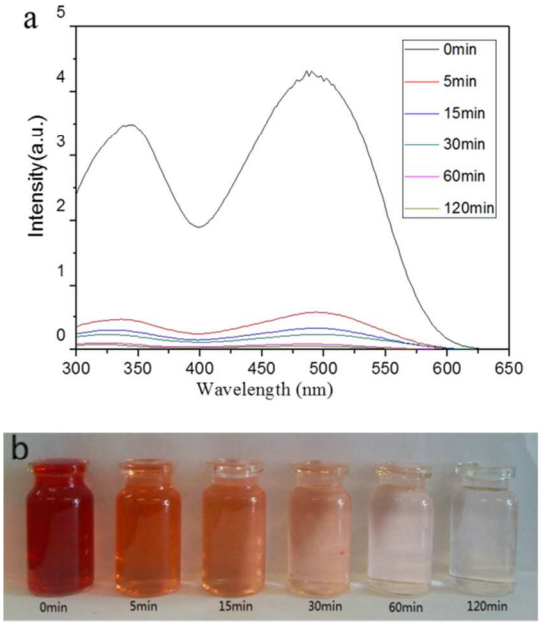

Fig. 5 (a) Absorption spectra and (b) photographs of 200 mL CR aqueous solution (300 mg L^{-1}) in the presence of 100 mg of MAS powder in different time.

some diffraction peaks of compounds of magnesium hydroxides and aluminium hydroxides appeared after adsorption. This indicated that the MAS samples were hydrolyzed into metal hydroxides in the water. Because the point of zero charge (PZC) of the MAS sample was around 11.8,[39] in neutral solution the MAS surface was positively charged, while the Congo red was negatively charged. Thus, the CR was easily adsorbed on the surface of the MAS due to the electrostatic attraction. In addition, the pH value of the solution was nearly invariant, which indicated that the metal hydroxides produced in the adsorption were stable.

Influence of some conditions, including adsorption time, initial concentration, initial pH and calcined temperature of the MAS, was investigated to explore the characteristics of the adsorption process. Adsorption property of the MAS powder for CR were characterised in ambient temperature and a dosage of 0.5g MAS powder per litre solution. Moreover, the conditions about MAS powder (calcination at 700 °C), the initial concentration (300mg L^{-1}) and pH value (7) of the CR solution were fixed for further ingestigation of other variable parameters. The time profile of CR adsorption at different initial concentrations with 0.5 g L^{-1} of the MAS powder is shown in Fig. 6a. Obviously, the adsorption rates of the MAS powder were extremely rapid during the first 5 min, and the adsorption process nearly reached equilibrium within 30 min under all concentrations. This indicated that the MAS powder was high efficiency for the removal of CR in aqueous solution. Fig. 6b shows the change tendency of adsorption capacity varying with the initial concentration. Strikingly, the adsorption capacities increased with the initial CR concentrations. It is because that higher concentration can provide greater driving force to prompt the CR diffusion to the MAS samples. As can be seen, when the initial concentration was greater than 450 mg L^{-1}, the increase of adsorption capacity became slow. This indicated that the adsorption was close to saturation when the initial concentration is 450 mg L^{-1}, and the max adsorption capacity of

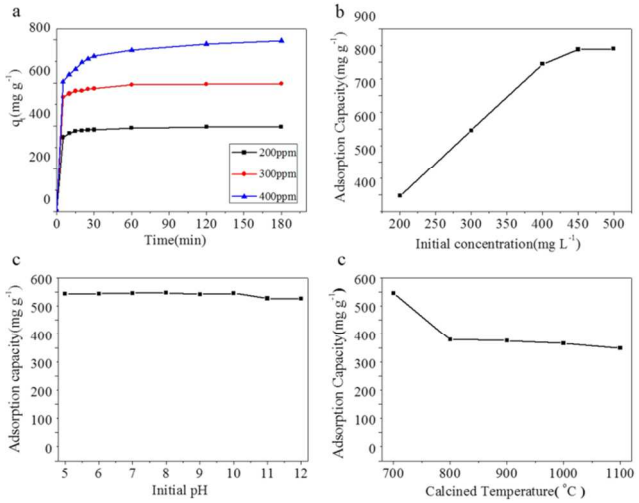

Fig. 6 Adsorption capacity of the MAS powder for CR removal with the changes of (a) the contact time, (b) the initial concentration, (c) initial pH and (d) calcined temperature.

the MAS samples was nearly 840 mg g^{-1}. Fig. 6c shows the influence of the initial pH on the CR adsorption of the MAS powder. At pH ranging from 5 to 10, the adsorption capacity was nearly invariant. With further increase of pH to 11.0, the adsorption capacity of the MAS powder decreased slightly. As well known, the MAS samples had a positive potential in a wide range of pH from 2.0 to 10, with a point of zero charge (PZC) around pH 11.8.[34] Thus, the positively charged CR was easily adsorbed on the surface of the MAS due to the electrostatic attraction. However, the absorption capacities of the MAS samples were still very high when the initial solution pH was beyond 12. It indicates that other interactions between the MAS samples and CR may exist during the adsorption. The interaction may be the coordination effect of magnesium ions and aluminium ions with amine groups and sulfo groups of Congo red. According to some previous reports, the coordination effect existed in the CR adsorption process when magnesia and alumina were used as absorbent. [5, 40, 41] The absorption capacity of the MAS powder calcined at different temperature is shown in the Fig. 6d. As can be seen, absorption capacities of the MAS powders decreased with the calcined temperature. The weaker electrostatic attraction resulted by more stable phase, and lower specific surface area of the absorbents with the increasing temperature leaded to the decrease of absorption capacity. It is worth noting that the decrease of the adsorption capacity from 700 °C to 800 °C was more obvious than the decrease at other temperatures. The crystallinity of the MAS calcined at 800 °C was much higher than that calcined at 700 °C, which resulted in much weaker hydrolysis and electrostatic attraction. Thus, more obvious decrease of the adsorption capacity appeared from 700 °C to 800 °C.

To explore the mechanism of the adsorption process, the pseudo-first-order, pseudo-second-order kinetic and intraparticle diffusion models were used to investigate the kinetics of CR adsorption on the MAS powder, respectively:

$$\log(q_e - q_t) = \log q_e - \frac{k_1 t}{2.303} \quad (1)$$

$$\frac{t}{q_t} = \frac{1}{k_2 q_e^2} + \frac{t}{q_e} \quad (2)$$

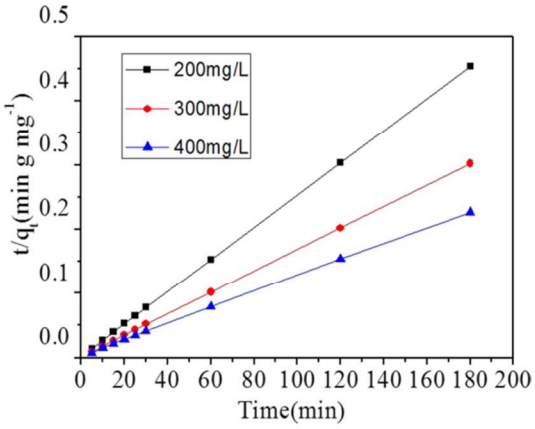

Fig. 7 The pseudo-second-order kinetics plots of CR adsorption on the as-prepared MAS powder.

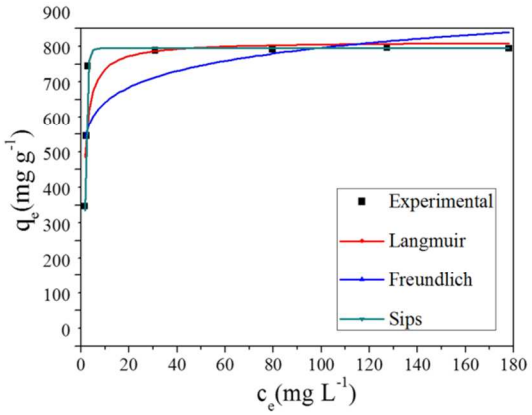

Fig. 8 Adsorption isotherm curves for the adsorption of CR on the as-prepared MAS powder.

$$q_t = k_3 t^{1/2} + C \quad (3)$$

Where q_e and q_t (mg g^{-1}) are the amounts of CR adsorbed at equilibrium and at any time t (min), respectively. k_1 (min^{-1}) and k_2 (g mg^{-1} min^{-1}) are the pseudo-first-order and pseudo-second-order rate constants, respectively. k_3 (mg g^{-1} $min^{-1/2}$) is the intraparticle diffusion rate constant and C (mg g^{-1}) is the constant. The kinetic parameters and the correlation coefficients (R^2) are summarized in Table S2 (†ESI). As can be obtained from Fig. 7 and Table S2, all the experimental data can match well to the pseudo-second-order model with high correlation coefficients (R^2 > 0.9998). Moreover, the values of $q_{e,cal}$ (q_e obtained by calculation) were very close to the values of $q_{e,exp}$ (q_e obtained by experiment). In contrast, the correlation coefficients for the pseudo-first-order model and intraparticle diffusion model were relatively lower, and the $q_{e,cal}$ of the pseudo-first-order model was more different with the $q_{e,exp}$. In conclusion, it is suitable to use the pseudo-second-order model to describe the adsorption process of CR on the as-prepared MAS powder. This indicated that the "surface reaction'' was a predominant factor and controlling stage for the CR removal.[42]

Fig. 8 shows the adsorption isotherms of CR on the as-prepared MAS powder at different initial concentrations. This adsorption process was analyzed using the Langmuir, Freundlich and Sips isotherm models, respectively.

$$q_e = \frac{q_m b C_e}{1 + b C_e} \quad (4)$$

$$q_e = K_f C_e^{1/n} \quad (5)$$

$$q_e = \frac{q_m (K_s C_e)^\gamma}{1 + (K_s C_e)^\gamma} \quad (6)$$

Where q_m (mg g^{-1}) is monolayer adsorption capacity, b is the Langmuir equilibrium constant (L mg^{-1}), K_f is roughly an indicator of the adsorption capacity, n is the adsorption intensity, K_s is the Sips equilibrium constant (L mg^{-1}), and γ is the Sips parameter. The related parameters and the correlation coefficients (R^2) are summarized in Table S3 (†ESI). The adsorption data were found to fit better to the Sips model, with R^2 value of 0.9738, than to the Langmuir and Freundlich models, with R^2 value of 0.6995 and 0.4958 respectively, suggesting the monolayer and nonuniform adsorption of CR on as-prepared MAS powder. The nonuniform distribution of the Mg^{2+} and Al^{3+} on the surface of the MAS spinel caused the nonuniformity of the absorbent, which further leaded to nonuniform chemical adsorption.

The change in free energy ΔG^0 (kJ mol^{-1}) for the adsorption process in the natural condition was estimated by using the following equation:

$$\Delta G^0 = -RT\ln K_S \quad (7)$$

Where T is the natural adsorption temperature (298.15 K), R is the ideal gas constant (8.314 J mol^{-1} K^{-1}). The value of the ΔG^0 estimated was 15.81 kJ mol^{-1}. The negative ΔG^0 indicated that CR adsorption on the MAS samples was spontaneous and feasible in the natural temperature.

Nowadays, many porous adsorbents have been proposed as candidates for the removal of CR, however, their adsorption capacities are normally below 500 mg g^{-1}. The adsorption capacity of as-prepared MAS powder and some other adsorbent previously used for removal of CR in aqueous solution is compared in Table 2. Obviously, the adsorption capacity of as-prepared MAS powder was higher than bulk MAS powder because the MAS powder had higher specific surface area. Moreover, adsorption capacity of MAS powder was higher than many other adsorbents. Strong interaction between the MAS powder and CR was the main reason for this fact.

Based on the above analysis, the adsorption of the CR solution mainly depends on the electrostatic attraction, as well as the coordination effect of the aluminium ions and magnesium ions with amine groups and the sulfo groups of the Congo red. Moreover, the powerful ability of as-prepared MAS samples to absorb CR was mainly owed to their strong interactions with the CR and their advantageous structure, including high specific surface area, large pore volume and uniquely hierarchical morphology.

Reusability is one of the most significant properties of the absorbent, and reusability of as-prepared MAS powder was evaluated. The XRD patterns for MAS calcined at 700 °C, 2-MAS and 3-MAS samples are shown in Fig. S7 (†ESI). As can be seen, the crystal phase and crystallinity of three samples were similar. It reveals that the crystal phase and crystallinity of the samples can be maintained in the cyclic process. Fig .S8 (†ESI) shows the N_2 ad/desorption isotherms of 2-MAS and 3-MAS samples. The isotherms can be classified as type II and H3 type hysteresis for both samples (according to the IUPAC classification), which were the same as the MAS sample calcined at 700 °C. The values of surface area for the 2-MAS and 3-MAS samples were 166.2 m^2 g^{-1} and 149.0 m^2 g^{-1} respectively, which were higher than the MAS sample calcined at 700 °C (127.9 m^2 g^{-1}). It is likely that the process of CR burned produced some pores in the samples resulting in increasing surface area of the samples. Meanwhile, the framework of the sample may be destroyed slightly in the calcinations, which can be used to explain the phenomenon that surface area of the 3-MAS sample was lower than the 2-MAS sample.

Table 2 Comparisons of CR adsorption capacities of different adsorbents

Adsorbent	Specific surface area m^2 g^{-1}	Removal capacity (mg g^{-1})	References
MAS sample	127.9	845.5	This work
Bulk MAS sample	73.2	322	This work
Mesoporous MgO architectures	94	689.7	4
MgO nanoplates	198	131.3	28
Spindle-like γ-Al_2O_3	149	176.7	29
Nanorod-like γ-Al_2O_3	158	83.8	30
NiO nanospheres	222	440	31
Urchin-like α-FeOOH	96.9	275	32

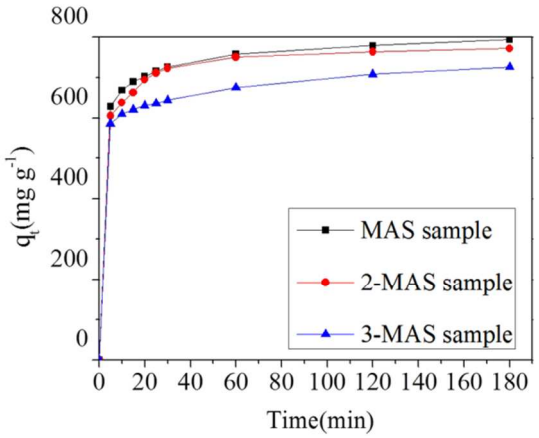

Fig. 9 Adsorption capacity of the MAS, 2-MAS and 3-MAS samples for CR removal with the changes of the contact time.

The time profile of CR adsorption at 400 mg L^{-1} initial concentrations with 0.5 g L^{-1} of the MAS, 2-MAS and 3-MAS powder is shown in Fig. 9. The adsorption rates of three samples were all rapid and the adsorption capacities of them declined successively, because the active sites of the absorbents decreased in the calcinations process. However, decrement of the adsorption capacity was little, and the adsorption capacity of the 3-MAS was nearly 720 mg g^{-1} in the CR solution (400 mg L^{-1}), which was still high. In conclusion, the combined superiority of the simple preparation, high adsorption rate, ultrahigh adsorption capacity and good reusability makes as-prepared MAS powder potential for application in environmental remediation.

4. Conclusion

In summary, we have demonstrated a simple route to prepare porous $MgAl_2O_4$ powder with $Mg_5(OH)_2(CO_3)_4{\cdot}4H_2O$ as a hard

template. The as-prepared MAS samples had hierarchical porous structure and large surface area. The MAS powder was high efficiency for the removal of CR in aqueous solution and the adsorption properties were systematically investigated. The kinetics and isotherm of adsorption process were proved to fit the pseudo-second-order kinetics and Sips isotherm models, respectively. The as-prepared MAS powder is potential for application in environmental remediation for its superior performance of removal organic dye.

Acknowledgements

This work was supported by National Natural Science Foundation of China (21276046, 21406032 and 21406045), the Fundamental Research Funds for the Central Universities of China (DUT13RC(3)043 and DUT14RC(3)040), the Ministry of Education Science and technology research projects and High-Tech R&D projects in Magnesium Industry of Liaoning Province in China.

Notes and references

State Key Laboratory of Fine Chemicals and School of Chemical Engineering, Dalian University of Technology, 2 Linggong Road, Dalian 116012, P. R. China. Fax: +86-0411-84986065 Tel: +86-0411-84986065 E-mail: ninggl@dlut.edu.cn;

† Electronic Supplementary Information (ESI) available: EDX, powder XRD pattern and N_2 ad/desorption isotherms of as-prepared MAS samples, and Kinetics parameter and Isotherm parameters for the adsorption of Congo red on MAS powder . See DOI: 10.1039/b000000x/

1 G. Crini, *Bioresource Technol.*, 2006, **97**, 1061-1085.
2 A. Mahapatra, B. G. Mishra and G. Hota, *Ceram. Int.*, 2013, **39**, 5443-5451.
3 P. Tian, J. W. Ye, G. L. Ning, W. T. Gong, N. Xu, Q. S. Zhang and Y. Lin, *RSC Adv.*, 2012, **2**, 10217-10221.
4 L. H. Ai, H. T. Yue and J. Jiang, *Nanoscale*, 2012, **4**, 5401-5408.
5 P. Tian, X. Y. Han, G. L. Ning, H. X. Fang, J. W. Ye, W. T. Gong and Y. Lin, *ACS Appl. Mater. Inter.*, 2013, **5**, 12411-12418.
6 D. Pant, A. Singh, G. Van Bogaert, S. Irving Olsen, P. Singh Nigam, L. Diels and K. Vanbroekhoven, *RSC Adv.*, 2012, **2**, 1248-1263.
7 H. Pang, W. Wang, Z. Yan, H. Zhang, X. Li, J. Chen, J. Zhang and B. Zhang, *RSC Adv.*, 2012, **2**, 9614-9618.
8 G. D. Nuernberg, E. L. Foletto, L. F. Probst, C. E. Campos, N. L. Carreño and M. A. Moreira, *Chem. Eng. J.*, 2012, **193**, 211-214.
9 I. Ganesh, *Int. Mater. Rev.*, 2013, **58**, 63-112.
10 W. Z. Li, L. Kovarik, D. H. Mei, J. Liu, Y. Wang and C. Peden, *Nat. Commun.*, 2013, **4**.
11 Y. Liu, S. Wang, D. N. Gao, T. J. Sun, C. X. Zhang and S. D. Wang, *Fuel Process. Technol.*, 2013, **111**, 55-61.
12 R. Feng, H. A. Al-Megren, M. C. Al-Kinany, M. J. Rood and Z. F. Yan, *J. Porous Mat.*, 2013, **20**, 571-577.
13 G. B. Nuernberg, E. L. Foletto, L. Probst, N. Carreno and M. A. Moreira, *J. Mol. Catal. A-Chem.*, 2013, **370**, 22-27.
14 E. L. Foletto, S. L. Jahn and R. Moreira, *Sep. Sci. Technol.*, 2009, **44**, 2132-2145.
15 B. Ismail, S. T. Hussain and S. Akram, *Chem. Eng. J.*, 2013, **219**, 395-402.
16 N. Hadian and M. Rezaei, *Fuel*, 2013, **113**, 571-579.
17 A. Laobuthee, S. Wongkasemjit, E. Traversa and R. M. Laine, *J. Eur. Ceram. Soc.*, 2000, **20**, 91-97.
18 J. Li, T. Ikegami, J. Lee, T. Mori and Y. Yajima, *Ceram. Int.*, 2001, **27**, 481-489.
19 M. F. Zawrah, H. Hamaad and S. Meky, *Ceram. Int.*, 2007, **33**, 969-978.
20 M. M. Rashad, Z. I. Zaki and H. El-Shall, *J. Mater. Sci.*, 2009, **44**, 2992-2998.
21 C. Păcurariu, I. Lazău, Z. Ecsedi, R. Lazău, P. Barvinschi and G. Mărginean, *J. Eur. Ceram. Soc.*, 2007, **27**, 707-710.
22 G. Ye, G. Oprea and T. Troczynski, *J. Am. Ceram. Soc.*, 2005, **88**, 3241-3244.
23 T. Shiono, H. Ishitomi, Y. Okamoto and T. Nishida, *J. Am. Ceram. Soc.*, 2000, **83**, 645-647.
24 Y. Yuan, S. R. Zhang and W. You, *J. Sol-Gel. Sci. Techn.*, 2004, **30**, 223-227.
25 P. Tian, J. Ye, N. Xu, W. Gong, Q. Zhang, Y. Lin and G. Ning, *Chem. Commun.*, 2011, **47**, 12008-12010.
26 Q. S. Zhang, J. W. Ye, P. Tian, X. Y. Lu, Y. Lin, Q. Zhao and G. L. Ning, *RSC Adv.*, 2013, **3**, 9739-9744.
27 X. Y. Han, P. Tian, H. C. Pang, Q. Song, G. L. Ning, Y. H. Yu and H. X. Fang, *RSC Adv.*, 2014, **4**, 28119-28125.
28 J. Hu, Z. Song, L. Chen, H. Yang, J. Li and R. Richards, *J. Chem. Eng. Data.*, 2010, **55**, 3742-3748.
29 W. Cai, J. Yu and M. Jaroniec, *J. Mater. Chem.*, 2010, **20**, 4587-4594.
30 W. Cai, Y. Hu, J. Chen, G. Zhang and T. Xia, *CrystEngComm*, 2012, **14**, 972-977.
31 T. Zhu, J. S. Chen and X. W. D. Lou, *J. Phys. Chem. C*, 2012, **116**, 6873-6878.
32 B. Wang, H. Wu, L. Yu, R. Xu, T. Lim and X. W. David Lou, *Adv. Mater.*, 2012, **24**, 1111-1116.
33 E. H. Walker Jr, J. W. Owens, M. Etienne and D. Walker, *Mater. Res. Bull.*, 2002, **37**, 1041-1050.
34 J. Guo, H. Lou, H. Zhao, X. Wang and X. Zheng, *Mater. Lett.*, 2004, **58**, 1920-1923.
35 O. R. Evans, A. T. Bell and T. D. Tilley, *J. Catal.*, 2004, **226**, 292-300.
36 T. Selvamani, A. Sinhamahapatra, D. Bhattacharjya and I. Mukhopadhyay, *Mater. Chem. Phys.*, 2011, **129**, 853-861.
37 C. M. Janet, B. Viswanathan, R. P. Viswanath and T. K. Varadarajan, *J. Phys. Chem. C*, 2007, **111**, 10267-10272.
38 H. B. Bafrooei and T. Ebadzadeh, *Ceram. Int.*, 2013, **39**, 8933-8940.
39 T. Kadosh, Y. Cohen, Y. Talmon and W. D. Kaplan, *J. Am. Ceram. Soc.*, 2012, **95**, 3103-3108
40 Y. Wang, W. Li, X. L. Jiao and D. R. Chen, *J. Mater. Chem. A,* 2013, **1**, 10720-10726.
41 J. Fei, Y. Cui, X. Yan, W. Qi, Y. Yang, K. Wang, Q. He and J. Li, *Adv. Mater.*, 2008, **20**, 452–456.
42 C. Y. Han, H. Y. Li, H. P. Pu, H. L. Yu, L. Deng, S. Huang and Y. M. Luo, *Chem. Eng. J.*, 2013, **217**, 1-9.